Quantifying and contextualising cyclone-driven, extreme flood magnitudes in bedrock-influenced dryland rivers

GEORGE HERITAGE[1], NEIL ENTWISTLE[2], *DAVID MILAN[3], STEPHEN TOOTH[4]

[1] AECOM, Exchange Court, 1 Dale Street, Liverpool, L2 2ET, UK

(George.Heritage@Aecom.com)

[2] University of Salford, Peel Building, University of Salford, Salford, M5 4WT, UK

(n.s.entwistle@salford.ac.uk)

[3] School of Environmental Sciences, University of Hull, Cottingham Road, Hull, HU6 7RX, UK

(d.milan@hull.ac.uk)

[4] Department of Geography and Earth Sciences, Aberystwyth University, Llandinam Building, Penglais Campus, Aberystwyth, SY23 3DB, UK (set@aber.ac.uk)

Abstract

In many drylands worldwide, rivers are subjected to episodic, extreme flood events and associated sediment stripping. These events may trigger transformations from mixed bedrock-alluvial channels characterised by high geomorphic and ecological diversity towards more dominantly bedrock channels with lower diversity. To date, hydrological and hydraulic data has tended to be limited for these bedrock-influenced dryland rivers, but recent advances in high-resolution data capture are enabling greater integration of different investigative approaches, which is helping to inform assessment of river response to changing hydroclimatic extremes. Here, we use field and remotely sensed data along with a novel 2D hydrodynamic modelling approach to estimate, for the first time, peak discharges that occurred during cyclone-driven floods in the Kruger National Park, eastern South Africa, in January 2012. We estimate peak discharges in the range of 4470 to 5630 m^3s^{-1} for the Sabie River (upstream catchment area 5715 km^2) and 14 407 to 16 772 m^3s^{-1} for the Olifants River (upstream catchment area 53 820 km^2). These estimates place both floods in the extreme category for each river, with the Olifants peak discharge ranking among the largest recorded or estimated for any southern African river in the last couple of hundred years. On both rivers, the floods resulted in significant changes to dryland river morphology, sediment flux and vegetation communities. Our modelling approach may be transferable to other sparsely gauged or ungauged rivers, and to sites where palaeoflood evidence is preserved. Against a backdrop of mounting evidence for global increases in hydroclimatic extremes, additional studies will help to refine our understanding of the relative and synergistic impacts of high-magnitude flood events on dryland river development.

Key words: dryland river, 2D hydraulic modelling, extreme flood, flood estimation, palaeoflood, Sabie River, Olifants River

INTRODUCTION

Drylands (hyperarid, arid, semiarid and dry-subhumid regions) cover 40-50% of the Earth's surface and sustain 30-40% of the world's population (e.g. United Nations, 2016). Many drylands are characterised by strong climatic variations, with extended dry periods interspersed with short, intense rainfall events, and are widely considered to be among the regions most vulnerable to future climate change (Obasi 2005; IPCC 2007; Wang et al., 2012). Many dryland river flow regimes are similarly variable (McMahon et al., 1992), with long periods of very low or no flow being followed by infrequent, short-lived, large or extreme flood events (see Tooth, 2013). This variable flow regime is one of the primary controls on dryland river process and form, commonly resulting in channel-floodplain morphologies and dynamics that differ markedly from many humid temperate rivers (Tooth, 2000, 2013; Jaeger et al., 2017). In particular, the role of extreme events in the episodic 'stripping' of unconsolidated alluvium from an underlying bedrock template has been reported as a key control on the long-term development of many southern African, Australian, Indian and North American dryland rivers (e.g. Womack and Schumm 1977; Baker 1977; Kale et al. 1996; Bourke and Pickup 1999; Rountree et al. 2000; Tooth and McCarthy 2004; Milan et al., 2018a, b). These stripping events limit long-term sediment build-up and contribute to incremental channel incision, which over many millennia leads to progressive valley deepening.

Over the last few decades, research into bedrock-influenced, dryland rivers has increased (e.g. Heritage et al., 1999, 2001; Tooth et al., 2002, 2013; Meshkova and Carling, 2012; Keen-Zebert et al., 2013), but hydrological and hydraulic data remain limited owing to the difficulty in collecting information in these typically harsh environments with their relatively infrequent channel-shaping flows. In particular, gauging stations commonly fail to accurately record flow data during large or extreme flood events, as the structures are commonly drowned out and/or suffer physical damage. This paucity of data hampers efforts to develop and apply conceptual and quantitative models of the response of these types of dryland rivers to past, present and future climatic changes, including the

relative and synergistic impacts of different floods on river morphology, sediment flux, and ecology (e.g. Milan et al., 2018b). Against a backdrop of heightening concern and mounting evidence for increases in hydroclimatic extremes in a warming world (e.g. Hansen et al., 2016: Steffen et al., 2018), these are critical gaps that limit our ability to manage such dryland rivers.

Woodward et al.'s (2010) overview of advances in flood and palaeoflood studies drew attention to alternative approaches to extracting hydrological and hydraulic information from fluvial environments where direct measurements are difficult or impossible. Among these approaches, computational modelling has led to significant insights into the flow hydraulics, sediment dynamics and morphological and ecological responses of fully alluvial rivers (e.g. Nicholas, 2005, 2010; Milan and Heritage, 2012) but to date there have not been similar advances in our understanding of bedrock-influenced, dryland river dynamics. For instance, owing to the paucity of channel roughness information available for these morphologically-diverse river types, past experience has shown that modelling and indirect estimation of extreme discharges commonly is problematic and may generate unreliable data (Broadhurst et al., 1997).

Despite these limitations, improved remote survey technologies (see Entwistle et al., 2018) and more sophisticated hydraulic modelling software now enhance the possibility of capturing and processing high-resolution topographic data to generate improved estimates of flood hydraulics and magnitudes in bedrock-influenced, dryland systems. In this paper, we demonstrate how a combination of field and remotely sensed data (e.g. aerial photography, Light Detection and Ranging (LiDAR)) has been used to apply a 2D hydraulic model for extensive (50 km long) reaches of the bedrock-influenced Sabie and Olifants rivers in the Kruger National Park (KNP), South Africa (Fig. 1), where Cyclone Dando generated high-magnitude floods in January 2012. As with high-magnitude, cyclone-generated floods in earlier decades (e.g. Cyclone Eline floods in January/February 2000), these 2012

floods had significant impacts on river geomorphology and ecology (Heritage et al., 2014; Milan et al., 2018b), and also on domestic and tourism infrastructure within and outside the KNP (Fitchett et al., 2016). Until now, however, reliable estimates of the peak flood magnitudes have been limited, particularly for the Olifants River along which extensive vegetation removal, alluvial stripping and infrastructural damage occurred. Our 2D modelling approach represents a step forward from previous flood magnitude estimation work in the KNP that employed 1D modelling and tended to focus mainly on the Sabie River alone or shorter reaches of other KNP rivers (e.g. Heritage et al., 2004). Our modelling approach may be transferable to other sparsely gauged or ungauged bedrock-influenced, dryland rivers that are subject to high-magnitude flood events, and to sites where palaeoflood evidence is preserved, and so may help to refine our understanding of the magnitude, frequency and impacts of such events on dryland river development. Hence, the aims of this paper are to: 1) use this 2D hydraulic model to estimate, for the first time, the peak discharges for the 2012 floods on the Sabie and Olifants rivers; 2) compare these estimates with those generated by other commonly-used flood estimation approaches; 3) compare the estimates with the peak discharges of large or extreme floods recorded or estimated previously on the KNP and other southern African rivers; and 4) outline the implications of changes to extreme flood magnitude and frequency for the development of the KNP rivers and other bedrock-influenced, dryland rivers globally.

STUDY SITES

The Sabie and Olifants rivers are located in the southern and central part of the KNP in the Mpumalanga and Limpopo provinces of northeastern South Africa (Fig. 1). The 54 570 km^2 Olifants catchment incorporates parts of the Highveld Plateau (2000-1500 m.a.s.l.), the Drakensberg Escarpment, and the Lowveld (400-250 m.a.s.l.). The 6320 km^2 Sabie River catchment covers part of the Drakensberg Mountains (~1600 m.a.s.l.), the low-relief Lowveld (~400 m.a.s.l.), and the Lebombo zone (~200 m.a.s.l.). Rainfall in both catchments is greater in the headwaters (2000 mm yr^{-1}) and declines rapidly eastwards towards the South Africa–Mozambique border (450 mm yr^{-1}).

Within the middle reaches, sediment is dominantly sand and fine gravel (median grain size 1-2 mm) (Broadhurst et al. 1997). Although water abstractions have altered the low flows (generally below 50 m^3s^{-1}) along both rivers, the intermittent, cyclone-driven flood flows are unaffected, and the channels remain unimpacted by engineering structures or other human activities over considerable lengths within the KNP. Thus, both rivers represent excellent, near-pristine sites for investigating bedrock-influenced, dryland river dynamics.

Fig. 1

In the KNP, both rivers are characterised by a bedrock 'macrochannel', which extends across the floor of a 10-20 m deep, incised valley. The macrochannel hosts one or more narrower channels, bars, islands and floodplains (Fig. 2A-C). Outside of the macrochannel, floods have a very infrequent and limited influence. These rivers are characterised by a high degree of bedrock influence, and the diverse underlying geology results in frequent, abrupt changes in macrochannel slope and associated sediment deposition patterns. Locally, bedrock may be buried by alluvial sediments of varying thickness, resulting in diverse channel types that range from fully alluvial (Fig. 2A) to more bedrock-influenced (Fig. 2B-C) (van Niekerk et al. 1995).

Fig. 2

In mid January 2012, Cyclone Dando impacted on eastern southern Africa. Widespread heavy rainfall (450-500 mm in 48 hours) led to high magnitude floods along many of the rivers that drain into and through the KNP. Preliminary 2D hydraulic modelling of the Sabie River floods (Heritage et al. 2014; Milan et al. 2018b) shows that local velocities peaked at 4 m s^{-1}, resulting in extensive vegetation removal, erosion and sedimentation along many reaches (Figs 2D-E). Here, we extend

our analyses of the 2012 floods, focusing on the use of a novel 2D hydrodynamic modelling approach to estimate the peak discharges along both the Sabie and Olifants rivers.

METHODS

Application of a 2D hydrodynamic model requires baseline data on channel topography in the form of a Digital Elevation Model (DEM). Following the Cyclone Dando floods in January 2012, aerial LiDAR and photography (Milan et al., 2018c) were obtained on 30th May 2012 for 50 km long reaches of both the Sabie and Olifants rivers in the KNP (Fig. 1). Southern Mapping Geospatial surveyed the rivers using an Opetch Orion 206 LiDAR, flown from a Cessna 206 at 1100 m altitude. Average point density was 409 318 points/km^2. The root mean squared error for z was 0.04 m, and for x and y was 0.06 m. Standard deviation for x and y were 0.05 and 0.06 m respectively, based on 5 ground survey points. These data effectively represent the post-flood condition of the rivers, both of which had suffered extensive vegetation and alluvial stripping, in many instances down to bedrock (e.g. Fig. 2D). Stripping likely would have occurred up to the peak flood flow and as such these stripped surfaces would be representative of the surfaces that experienced the maximum discharges being estimated in this study.

Strandline elevations

At selected sites along the Sabie and Olifants rivers, the flow levels associated with the Cyclone Dando floods were surveyed using a Leica 500 RTK GPS in May 2012 (Figs 1B-C). Despite the four months that had elapsed between the January floods and the surveys (a time gap imposed by the availability of funding), strandlines of organic debris (e.g. branches, twigs, reeds) were very well preserved along significant lengths of each survey reach (Figs 2E-G). The fresh condition of the debris and occasional ‘best before’ dates on embedded plastic bottles showed clearly that these strandlines were from the January 2012 floods (Fig. 2H).

Previous work (Heritage et al., 2004; Fisher, 2005) has shown that receding floods can leave several strandlines depending on local conditions. Furthermore, elevation differences of 3 m were often evident between the base and top of individual strandlines, and some strandlines were measured in locations where debris was less abundant than the locations illustrated in Figures 2F-G. Nevertheless, surveys focused on finer organic material (e.g. see Fig. 2G), taking the highest elevation debris line as the datum within a given reach, and therefore provide an indication of the highest stage reached by the 2012 floods. Survey of larger woody debris (e.g. Fig. 2E) was avoided owing to uncertainties in determining actual water level arising from likely super-elevation of water surfaces and the flexibility of some woody elements (e.g. stems) in high flows.

Hydrodynamic modelling

The post-flood LiDAR data (Milan et al., 2018c) for the Sabie and Olifants rivers were used to provide the physical boundary conditions for hydraulic modelling of the 2012 floods. Our analyses represent the longest and most detailed flow simulations conducted on the rivers in the region, and generate hydraulic parameter estimates for the floods at 2 m scale along 50 km reaches in a single integrated model for each river. Flow resistance parameters are required to represent many sources of energy loss (Lane and Hardy, 2002). A Mannings 'n' or Darcy Weisbach *f* flow resistance value is most often used to represent grain roughness. Previous research protocols have used both a uniform parameter and spatially distributed parameterisation (Legleiter et al. 2011, Logan et al. 2011). Werner et al. (2005) demonstrated that spatially-distributed floodplain roughness failed to improve flood model performance when compared to use of a single roughness class. Horritt and Bates (2002) and Bates et al. (2006) also found that use of a constant channel and floodplain roughness value provided a pragmatic approach to flood modelling. They also noted that many of the roughness factors represented by the roughness coefficient in 1D models are integrated into the modelling process in 2D models, most notably form roughness. Form roughness includes the effects of projected

morphological units such as bars and bedrock islands into the flow, which is represented by topographic variation in the DEM and implicitly includes changes in channel type (e.g. Figs 2A-C) along each 50 km modelled reach. As such, no attempt was made to incorporate sophisticated representations of spatial roughness patterns based on factors such as sediment size variation or vegetation community patterns for the study reaches, with a nominal Manning's 'n' roughness value of 0.04 used in the simulations to represent model skin resistance (see Broadhurst et al., 1997).

Our analyses used JFlow, a 2-D depth-averaged flow model. JFlow is a commercial 2-D flow modeling tool noted for its ability to handle large data sets through the use of a graphics processing unit-based computation. JFlow was developed as a solution to harness the full detail of available topographic data sets such as those available from LiDAR, and to investigate overland flow paths (Bradbrook, 2006). Simplified forms of the full 2-D hydrodynamic equations are used in the model, but the main controls on flood routing for shallow, topographically driven flow are captured (Bradbrook, 2006). As such, JFlow simulations must be regarded as only a first approximation of 2-D flow but its ability to handle topographically induced form roughness (a major resistance component on the systems being studied) and its relatively rapid run time and robustness on long complex reaches makes it suitable for the proposed modelling. The model also performed well compared to other shallow water simulations in a benchmarking exercise by the Environment Agency in the UK (Néelz and Pender, 2013). Bates et al. (2010) and Neal et al. (2010) demonstrated that the model was capable of simulating flow depths and velocities within 10% of a range of industry full shallow water codes such as TuFlow and InfoWorks. The gradually varied flow simulations by Bates et al. (2010) revealed that velocity predictions were 'surprisingly similar' between the models and they suggest that JFlow model may be appropriate for velocity simulation across a range of gradually varied, subcritical flow conditions.

The DEMs of each study reach were degraded to uniform 1 m data grids and input into the JFlow software to generate 2 m resolution surface meshes using a uniform triangulation algorithm. Morphologic-scale form roughness variation (and by definition channel type) was defined using the local bed level variation derived from the original survey data (see Entwistle et al., 2014). We assume that at flow peak the majority of the alluvium and vegetation in the two rivers had been eroded, and as such their impacts on flow resistance were not considered. Inflow and outflow discharges and flow stage boundaries were set during hydraulic model runs, based on low flow survey data and high flow approximations (these were refined within the program during model runs to satisfy the conservation of mass and momentum equations). Flow simulations were conducted up to 5000 m^3s^{-1} on the Sabie River and up to 15 000 m^3s^{-1} on the Olifants River. These upper values were chosen based on a continuity equation estimate of peak flows, using field surveyed channel widths, depths, and assumed reach-average velocities. These data were used to develop simulated rating curves for each of the survey sites.

Flood estimation

Simulated water surface elevation versus simulated discharge rating curves were derived for the upstream and downstream parts of each of the sites shown in Figs 1B-C. These values were used to estimate peak flows using the surveyed RTK GPS strandline elevations.

RESULTS

Model validation

Comparisons were made between the simulated water surface elevations and the RTK GPS surveyed strandlines (Fig. 3). For the Sabie River (Fig. 3A), very close matches were found at sites 1, 2, 4 and 6, with RTK elevations mostly within 0.3 m of the simulated water elevations. Simulated water elevations are over-predicted by 0.5-1.5 m for sites 3 and 5, whereas simulated water elevations were

under-predicted by 1.0-1.5 m at sites 7 and 8 farther downstream. For the Olifants River (Fig. 3B), simulated water surfaces show much more variability but surveyed strandline elevations are generally within 1 m of the simulated elevations. The water surface simulation data suggest that the assumptions of gradually varied flow and subcritical flow are not always satisfied along the model reaches (Coulthard et al., 2013) and this will introduce a degree of error in the calculated discharges. For both rivers, the deviation between simulated and surveyed elevations was in the same order as the vertical variation (± 3 m) evident for the strandlines (Figs 3A-B). Some parts of the surveyed elevations along the strandlines matched simulated water elevations better than others, suggesting the possibility of multiple strandlines having been surveyed. Multiple strandlines may have resulted from pulsing on the rising or falling limb of the flood hydrographs but this cannot be verified owing to a lack of gauge data. Modelled and surveyed flood inundation extents are plotted in Figure 4. For the Sabie River, there is a very close match between modelled and surveyed inundation extents (Fig. 4A), whereas for the Olifants River, simulated inundation extent appears to be slightly under-predicted relative to the surveyed extent (Fig. 4B).

Fig. 3

Fig. 4

Extreme flood estimation

The flood stages for the 5000 m^3s^{-1} flow simulation for the sites along the Sabie River are lower in elevation than the majority of surveyed strandline elevations, especially along the lowermost sites (Fig. 3A), and do not exceed the limits of the surveyed inundation extents (Fig. 4A). This suggests that during the 2012 floods, peak discharges were slightly in excess of this simulated flow. Regression analysis-derived rating equations for each study site along the Sabie study reach (Fig. 1B) allowed estimation of the peak flood discharge, which ranges from 4470 m^3s^{-1} to 5630 m^3s^{-1} (Table

1, Fig. 5A). For the Sabie River, these results suggest that 2012 floods did not exceed the peak stage or extent of the 2000 Cyclone Eline floods, which ranged between 6000 and 7000 m^3s^{-1} towards the lower end of the Sabie study reach (Heritage et al., 2003). This conclusion is supported by field observations from the Sabie River. At the Low Level Bridge crossing near Skukuza (Fig. 1A), a roadside marker indicates the limit of the 2000 floods. This marker stands at a higher elevation than the strandlines from the 2012 floods, indicating that at this location, the 2012 floods were not as large as the 2000 floods. The anecdotal accounts of park rangers suggest that this finding also applies more widely along the Sabie study reach, and is supported by the absence of any damage during the 2012 floods to the tarred road that runs adjacent to the macrochannel margins along the right bank, whereas this road had been extensively damaged during the 2000 event.

Table 1

Fig. 5

The flood stages for the 15 000 m^3s^{-1} flood simulation for the sites along the Olifants River exceed some of the surveyed strandline elevations (Fig. 3B) but remains within the limits of the surveyed inundation extents (Fig. 4B). This suggests that during the 2012 floods, peak discharges approached or slightly exceeded this simulated flow. Regression analysis derived rating equations for each study site allowed estimation of the peak flood magnitude, which ranges from 14 407 m^3s^{-1} to 16 772 m^3s^{-1} depending on location (Table 1, Fig. 5B).

DISCUSSION

Comparisons between flood estimation methods

The method used in this paper to estimate flood magnitudes along the Sabie and Olifants rivers can

be compared to other published methods for estimating (palaeo)flood velocities and discharges. These methods range from the use of regime type equations (e.g. Wohl and David, 2008), maximum transported grain size and/or bedform dimensions (e.g. Costa, 1983; Williams, 1983; Wohl and Merritt, 2008), and friction based approaches (e.g. Kochel and Baker, 1982; Heritage et al., 1997; Broadhurst et al., 1997; Birkhead et al., 2000).

Wohl and David's (2008) width–discharge relationship for bedrock-influenced channels is statistically significant, but the r^2 value for the regime equation was low at 0.59, principally due to variation in rock strength. This relationship was applied to the study sites on the Sabie and Olifants rivers and generated peak flows of between 25 000 to 50 000 m^3s^{-1} for the Sabie (macrochannel width 250-500 m), and 75 000 m^3s^{-1} in wider reaches on the Olifants (macrochannel width 700 m). All but the lower values are outside the range of data used by Wohl and David (2008) to generate the original width–discharge relationship. As such, little confidence can be placed in the application of this regime type approach to estimating flood magnitude on the KNP rivers.

Application of the maximum transported grain size to derive an average flood velocity estimate (Costa, 1983; Williams, 1983) is also difficult to apply in the case of the Sabie and Olifants rivers. In both catchments, the metamorphic and igneous bedrock weathers to supply mainly sand and fine gravel (granules, minor pebbles) to the rivers. Consequently, cobble- or boulder-sized sediment is supply limited and any use of the empirical relationships would lead to a gross underestimation of peak velocities and associated discharges.

Application of the slope-area method to the downstream parts of the study reaches of both rivers using an estimated Darcy-Weisbach friction factor of 0.125 and a strandline-derived macrochannel water surface slope generated peak discharge estimates of between 3112 m^3s^{-1} and 3558 m^3s^{-1} for the Sabie River and between 12 923 m^3s^{-1} and 13 417 m^3s^{-1} for the Olifants River. These estimates are lower

than the peak discharge predicted using the 2D modelling approach and are likely to be less accurate as the slope-area method uses an average reach slope and estimated roughness coefficients derived from the strandline data and previously published research (Broadhurst et al., 1997; Birkhead et al., 2000). This contrasts with the 2D approach adopted here where the form roughness and water surface slope are intrinsically linked to the detailed local topographic variation captured in the baseline LiDAR DEM.

In summary, these alternative approaches to flood discharge estimation along the Sabie and Olifants rivers yield a wide variety of values, with some approaches clearly inapplicable or inappropriate given the context of the study sites. Even the more sophisticated approaches that utilise slope, area and friction data require many of these parameters to be estimated or are limited by difficulty in accurately measuring strandlines in the field.

The simplified 2D JFlow method applied in this study does not require such data and can estimate flood discharge from a detailed topographic model alone (e.g. a LiDAR-derived DEM). This model contains 'effective' parameters that are related to aggregated hydraulic processes, which cannot, in general, be determined from the physical characteristics of the reach under consideration (Hunter et al., 2007). Channel form roughness, capturing protrusion into the flow at the morphological unit scale (including sand bars and bedrock islands, which, when aggregated, also represent channel type differences – Fig. 2A-C), is explicitly integrated into the modelling approach through the detailed LiDAR-derived DEM. As outlined above, in our study a single representative grain and hydraulic flow resistance value was input to the model as this represents only a minor component of flow resistance. Stripping of vegetation and alluvium was also likely to have occurred up to the peak discharge, and as such the stripped DEM (i.e. that based on post-flood survey) was assumed to adequately represent the overall form resistance operating at the flood peak.

Previous research (e.g. Werner et al., 2005) supports this approach, demonstrating that spatially-distributed floodplain roughness based on land-use mapping failed to improve flood model performance when compared to use of a single floodplain roughness class. Horritt and Bates (2002) and Bates et al. (2006) also found that utilisation of a constant channel and floodplain roughness value provided a pragmatic approach to flood modelling. Such an approach is also justified on the grounds that the approach is primarily for use in estimating palaeofloods. As such, in these previous studies, no attempt was made to incorporate more sophisticated representations of spatial roughness pattern based on factors such as sediment size variation and vegetation community patterns, as these data are typically not available in palaeocontexts.

Comparisons with extreme floods on other southern African rivers

Based on the historic flow record (Fig. 6A), the 2012 Cyclone Dando floods on the Sabie River can be classed as 'extreme' but as noted above, these were of lower magnitude than the 2000 floods (Heritage et al., 2004). Based on the historic record (Fig. 6B), the 14 407 m^3s^{-1} to 16 772 m^3s^{-1} peak discharge estimate for the Olifants River 2012 floods appears to be more extreme. Indeed, in comparison with the catalogue of maximum peak discharges compiled by Kovacs (1988) and other related studies, these 2012 floods rank among some of the most extreme floods recorded for any southern African river in the last couple of hundred years (Fig. 7). For instance, the 2012 Olifants River peak discharge far exceeds the well-documented 1981 Buffels River flood of up to 8000 m^3s^{-1} (Stear, 1985; Zawada, 1994), the 1987 lower uMgeni River flood of 5000-10 000 m^3s^{-1} (Cooper et al., 1990; Smith, 1992) and the 1974 and 1988 discharges of 8000-9000 m^3s^{-1} that occurred along the much larger middle Orange River (du Plessis et al., 1989; Bremner et al., 1990; Zawada and Smith, 1991; Zawada, 2000). The 2012 Olifants River peak discharge is even comparable in magnitude to the extreme floods that occurred along rivers draining to the KwaZulu-Natal coast during Cyclone Domoina in January 1984 (Kovacs et al., 1985; Kovacs, 1988). Higher discharges

have almost undoubtedly occurred along much larger rivers such as the Orange earlier in the Holocene; for example, 13 palaeofloods with discharges in the range of 10 000-15 000 m^3s^{-1} occurred along the lower Orange River during the last 5500 years and were exceeded by one catastrophic discharge of around 28 000 m^3s^{-1} sometime between AD 1453 and AD 1785 (Zawada 1996; 2000; Zawada et al., 1996). Nevertheless, the 2012 Olifants River floods remain notable on an historic timescale, particularly given the associated geomorphological impacts, which involved widespread loss of vegetation and stripping of alluvium down to the underlying bedrock template along extensive reaches of the river in the KNP (Fig. 2D).

Fig. 6

Fig. 7

Implications of changes to extreme floods for bedrock-influenced, dryland river development

Although the Sabie and Olifants river 2012 floods can be classed as extreme, the peak discharges have been equalled or exceeded by floods on many other rivers globally (see compilation by Baker, 2006). When considered against catchment area, however, the 2012 floods fall within the cluster of extreme floods recorded in other global regions, including drylands such as the Colorado Plateau and Negev Desert, so still rank as significant. Indeed, the Sabie and Olifants 2012 floods resulted in significant changes to river morphology, ecology and infrastructure within and outside the KNP (Heritage et al., 2014; Fitchett et al., 2016; Milan et al., 2018b), especially as they occurred only 12 years after the Cyclone Eline floods. For the Sabie River specifically, Milan et al. (2018b) examined the relative and synergistic impacts of the 2000 and 2012 floods, and demonstrated that although the 2012 floods were of lower magnitude and overall had a more subdued morphological impact, significant erosion and deposition nonetheless occurred. In particular, in some subreaches, remnant

islands and large trees that survived the 2000 floods were removed during the subsequent 2012 floods owing to their wider exposure to flow (Milan et al., 2018b).

Indeed, along other KNP rivers and many other bedrock-influenced, dryland rivers across southern Africa and farther afield, flood sequencing is undoubtedly a key driver of river development, both geomorphologically and ecologically. Based on the Sabie River example, Milan et al. (2018b) proposed a conceptual model that incorporates flood sequencing, channel type, and sediment supply influences. They argue that following partial or complete stripping events, recovery to pre-flood, more alluvial, more vegetated conditions requires relatively long gaps (e.g. 20-30 years) between large or extreme floods, within which intervening smaller floods occur and conditions for vegetation re-establishment are favourable. Given evidence for increased rainfall quantities during wet seasons (MacFadyen et al., 2018) and climate change projections that indicate the potential for future increases in the frequency of cyclone-generated extreme floods in eastern southern Africa (Fitchett and Grab, 2014), however, it is possible that extreme flood magnitudes and frequencies on the KNP rivers will become increasingly common and the rivers may no longer experience prolonged periods of lower magnitude floods. Potentially, this could trigger state changes from the current dominance of mixed bedrock-alluvial channel types characterised by high geomorphic and ecological diversity (Figs 2A-B) towards more dominantly bedrock channels with limited volumes of transient alluvium and lower ecological diversity (Figs 2C-D). Such changes would have significant implications for ecosystem service delivery and associated river management strategies. In a world where hydroclimatic extremes such as floods and droughts may be increasing (Hansen et al., 2016; Steffen et al., 2018), similar changes may well occur along other bedrock-influenced rivers across the southern African drylands (e.g. Tooth and McCarthy, 2004) and also farther afield, including rivers in arid to semiarid central Texas, USA (e.g. Baker, 1977) and in subtropical wet-dry settings such as southeast Queensland, Australia (Croke et al., 2013; Baggs Sargood et al., 2015). Given the paucity of flood hydrological and hydraulic data along such rivers, however, these types of conceptual models

have yet to be fully quantified or tested but nonetheless provide a guide for anticipating possible future pathways of river development.

CONCLUSION

Recent decades have seen a growth in scientific studies of past and present floods (e.g. Saint-Laurent, 2004; Baker, 2006, 2008; Woodward et al., 2010) and the need for accurate estimation of flood magnitudes, frequencies and hydraulics is becoming of greater importance as climate change impacts on flow regimes across the globe. In particular, as Baker (2006) has noted, additional (palaeo)flood data are needed to test hypotheses of increases in extreme flooding and to enable incorporation into flood risk assessment. In this paper, we have used a simplified but novel 2D modelling approach to estimate the magnitudes of the cyclone-driven flood events on the Sabie and Olifants rivers in January 2012. The approach relies on an accurate LiDAR-derived DEM of a river to account for form roughness, assuming that vegetation and alluvial stripping had occurred prior to the flood peak, and applies a uniform additional roughness factor to account for grain and hydraulic flow resistance components. The use of a simplified 2D code allows for more rapid simulations, enables modelling of very long reaches in detail, and provides a robust modelling framework that can generate hydraulic estimates for a range of flows. Comparison of field surveyed and simulated water surface slope and inundation patterns for the peak flows suggests that the model performs well overall.

Our approach should be transferable to many other bedrock-influenced, flood-impacted, dryland rivers globally, and so potentially can make a contribution to improved documentation and analysis of one of the most pervasive global environmental hazards. On both the Sabie and Olifants rivers, the flood flows can be described as ‘extreme’, with the peak discharge on the Olifants being among one of the largest ever recorded or estimated for any southern African river in the late Holocene. Over the 50 km long study reach, the floods resulted in widespread loss of vegetation and extensive

stripping of alluvium down to the underlying bedrock template, demonstrating the importance of such system 'resetting' events in long-term river development. Under future scenarios where there is an increase in the magnitude and frequency of flood extremes along bedrock-influenced, dryland rivers, this may trigger a state change from more mixed bedrock-alluvial systems with relatively high geomorphological and ecological diversity towards more bedrock-dominated systems with lower diversity. If correct, such changes will have significant implications for ecosystem service delivery and associated river management strategies.

ACKNOWLEDGMENTS

This project was funded through NERC Urgency Grant NE/K001132/1. We would like to thank SANParks for supporting this research. JBA Consulting are acknowledged for allowing use of JFlow. Simon Sherrington is acknowledged for his preliminary help with data processing. We also thank the two anonymous reviewers and the journal editors (Paolo D'Odorico and Simon Papalexiou) for comments that helped us to refine our presentation of data and arguments.

REFERENCES

Baggs Sargood, M., Cohen, T.J., Thompson, C.J., Croke, J., 2015, Hitting rock bottom: morphological responses of bedrock-confined streams to a catastrophic flood. Earth Surface Dynamics 3, 265–279.

Baker, V.R., 1977. Stream-channel response to floods, with examples from central Texas. Geological Society of America Bulletin 88, 1057-1071.

Baker VR., 2006. Palaeoflood hydrology in a global context. Catena 66, 161-168.

Baker VR., 2008. Palaeoflood hydrology: origin, progress, prospects. Geomorphology 101, 1-13.

Bates, P.D., Wilson, M.D., Horritt, M.S., Mason, D.C., Holden, N., Currie, A., 2006. Reach scale floodplain inundation dynamics observed using airborne synthetic aperture radar imagery: Data analysis and modelling. Journal of Hydrology 328, 306-318.

Bates, P.D., Horritt, M.S. and Fewtrell, T.J., 2010. A simple inertial formulation of the shallow water equations for efficient two-dimensional flood inundation modelling. Journal of Hydrology, 387(1-2), pp.33-45.

Birkhead, A.L., Heritage, G.L., James, C.S., Rogers, K.H., van Niekerk, A.W., 2000. Geomorphological change models for the Sabie River in the Kruger National Park. Water Research Commission Report 782/1/00.

Bourke, M.C., Pickup, G., 1999. Fluvial form variability in arid central Australia. In: Miller, A.J., Gupta, A. (Eds), Varieties of Fluvial Form. Chichester: Wiley, pp. 249-271.

Bremner, J.M., Rogers, J., Willis, J.P., 1990. Sedimentological aspects of the 1988 Orange River floods. Transactions of the Royal Society of South Africa 47, 247–294.

Bradbrook, K., 2006. JFlow: a multiscale two-dimensional dynamic flood model. Water and Environment Journal, 20(2), pp.79-86.

Broadhurst, L.J., Heritage, G.H., van Niekerk, A.W., James, C.S, Rogers, K.H., 1997. Translating discharge into local hydraulic conditions on the Sabie River: an assessment of channel flow resistance. Water Research Commission Report 474/2/97.

Cooper, J.A.G., Mason, T.R., Reddering, J.S.V., Illenberger, W.K., 1990. Geomorphic effects of catastrophic flooding on a small estuary. Earth Surface Processes and Landforms 15, 25-41.

Costa, J.E., 1983. Paleohydraulic reconstruction of flash-flood peaks from boulder deposits in the Colorado Front Range. Geological Society of America Bulletin 94, 986-1004.

Coulthard, T.J., Neal, J.C., Bates, P.D., Ramirez, J., Almeida, G.A. and Hancock, G.R., 2013. Integrating the LISFLOOD‐FP 2D hydrodynamic model with the CAESAR model: implications for modelling landscape evolution. Earth Surface Processes and Landforms, 38(15), pp.1897-1906.

Croke, J., Todd, P., Thompson, C., Watson, F., Denham, R., Khanal, G., 2013. The use of multi temporal LiDAR to assess basin-scale erosion and deposition following the catastrophic January

2011 Lockyer flood, SE Queensland, Australia. Geomorphology 184, 111-126.

du Plessis, D.B., Dunsmore, S.J., Burger, C.E., Randall, L.A., 1989. Documentation of the February–March 1988 floods in the Orange River basin. Pretoria: Department of Water Affairs, Technical Report TR 142.

Entwistle, N.S., Heritage, G.L., Tooth, S., Milan, D., 2014. Anastomosing reach control on hydraulics and sediment distribution on the Sabie River, South Africa. Proceedings of the International Association of Hydrological Sciences 367, 215-219.

Entwistle, N., Heritage, G.L., Milan, D.J. 2018. Recent Remote Sensing Applications for Hydro and Morphodynamic Monitoring and Modelling. Earth Surface Processes and Landforms 43, 2283-2291.

Fisher, T.G., 2005. Strandline analysis in the southern basin of glacial Lake Agassiz, Minnesota and North and South Dakota, USA. Geological Society of America Bulletin 117, 1481-1496.

Fitchett, J.M., Hoogendoorn, G., Swemmer, A.M., 2016. Economic costs of the 2012 floods on tourism in the Mopani District Municipality, South Africa. Transactions of the Royal Society of South Africa 71, 187-194.

Hansen, J., Sato, M., Hearty, P., Ruedy, R., Kelley, M., Masson-Delmotte, V., Russell, G., Tselioudis, G., Cao, J., Rignot, E., Velicogna, I., Tormey, B., Donovan, B., Kandiano, E., von Schuckmann, K., Kharecha, P., Legrande, A.N., Bauer, M., Lo, K-W., 2016. Ice melt, sea level rise and superstorms: evidence from paleoclimate data, climate modeling, and modern observations that 2 °C global warming could be dangerous. Atmospheric Chemistry and Physics 16, 3761–3812.

Heritage, G.L., Large, A., Moon, B., Jewitt, G., 2004. Channel hydraulics and geomorphic effects of an extreme flood event on the Sabie River, South Africa. Catena 58, 151-181.

Heritage, G.L., Large, A.R.G., Moon, B.P., Birkhead, A.L., 2003. Estimating extreme flood magnitude in bedrock-influenced channels using representative reach-based channel resistance data. Geografiska Annaler: Series A, Physical Geography 85, 1-11.

Heritage, G.L., Moon, B.P., Jewitt, G.P., Large, A.R.G., Rountree, M., 2001. The February 2000

floods on the Sabie River, South Africa: an examination of their magnitude and frequency. Koedoe 44, 37–44.

Heritage, G.L., Tooth, S., Entwistle, N., Milan, D.J., 2014. Long-term flood controls on semi-arid river form: evidence from the Sabie and Olifants rivers, eastern South Africa. Proceedings of the International Association of Hydrological Sciences 367, 141-146.

Heritage, G.L., van Niekerk, A.W., Moon, B.P., 1999. Geomorphology of the Sabie River, South Africa: an incised bedrock-influenced channel. In: Miller, A.J., Gupta, A., (Eds.), Varieties of Fluvial Form: Wiley, Chichester, pp. 53–79.

Heritage, G.L., van Niekerk, A.W., Moon, B.P., Broadhurst, L.J., Rogers, K.H., James, C.S., 1997. The geomorphological response to changing flow regimes of the Sabie and Letaba river systems. Report-Water Research Commission, vol. 376/1/97. Pretoria, South Africa. 164 pp.

Horritt, M.S., Bates, P.D., 2002. Evaluation of 1D and 2D numerical models for predicting river flood inundation. Journal of Hydrology 268, 87-99.

Hunter, N.M., Bates, P.D., Horritt, M.S., Wilson, M.D., 2007. Simple spatially-distributed models for predicting flood inundation: a review. Geomorphology 90, 208-225.

IPCC, 2007. Climate Change 2007: Synthesis Report. Summary for Policymakers. IPCC.

Jaeger, K.L., Sutfin, N.A., Tooth, S., Michaelides, K., Singer, M., 2017. Geomorphology and sediment regimes of intermittent rivers and ephemeral streams. In: Datry et al. (Eds.), Intermittent Rivers and Ephemeral Streams: Ecology and Management, Elsevier, in press.

Kale, V.S., Baker, V.R., Mishra, S., 1996. Multi-channel patterns of bedrock rivers: an example from the central Narmada basin, India. Catena 26, 85–98.

Keen-Zebert, A., Tooth, S., Rodnight, H., Duller, G.A.T., Roberts, H.M., Grenfell, M., 2013. Late Quaternary floodplain reworking and the preservation of alluvial sedimentary archives in unconfined and confined river valleys in the eastern interior of South Africa. Geomorphology 185, 54-66.

Kochel, R.C., Baker, V.R., 1982. Paleoflood hydrology. Science 215, 53-361.

Kovacs, Z.P., 1988. Regional Maximum Flood Peaks in Southern Africa. Pretoria: Department of Water Affairs, Directorate of Hydrology, Technical Report 137.

Kovacs, Z.P., du Plessis, D.B., Bracher, P.R., Dunn, P., Mallory, G.C.L., 1985. Documentation of the 1984 Domoina floods. Pretoria: Department of Water Affairs, Technical Report TR 122.

Lane, S.N., Hardy, R.J., 2002. 16-Porous rivers: A new way of conceptualising and modelling river and floodplain flows? Transport Phenomena in Porous Media II, 425-449.

Legleiter, C.J., Kyriakidis, P.C., McDonald, R.R. and Nelson, J.M., 2011. Effects of uncertain topographic input data on two‐dimensional flow modeling in a gravel-bed river. Water Resources Research, 47.

Logan, B.L., McDonald, R.R., Nelson, J.M., Kinzel, P.J. and Barton, G.J., 2011. Use of multidimensional modeling to evaluate a channel restoration design for the Kootenai River, Idaho (No. 2010-5213, pp. i-68). US Geological Survey.

McMahon, T.A., Finlayson, B.L., Haines, A.T., Srikanthan, R., 1992. Global runoff: continental comparisons of annual flows and peak discharges. Catena Paperback. Cremlingen-Destedt.

MacFadyen, S., Zambatis, N., Van Teeffelen, A.J., Hui, C. 2018. Long-term rainfall regression surfaces for the Kruger National Park, South Africa: a spatio-temporal review of patterns from 1981 to 2015. International Journal of Climatology, 38: 2506-2519.

Meshkova, L.V., Carling, P.A., 2012. The geomorphological characteristics of the Mekong river in northern Cambodia: a mixed bedrock–alluvial multi-channel network. Geomorphology 147–148, 2–17.

Milan, D.J., Heritage, G.L., 2012. LiDAR and ADCP use in gravel bed rivers: Advances since GBR6. In Church, M., Biron, P., Roy, A., (Eds.), Gravel-bed rivers: Processes, Tools, Environments. John Wiley & Sons, Chichester, p. 286-302.

Milan, D., Heritage, G., Entwistle, N. and Tooth, S., 2018a. Morphodynamic simulation of sediment deposition patterns on a recently stripped bedrock anastomosed channel. Proceedings of the

International Association of Hydrological Sciences, 377, p.51.

Milan, D.J., Heritage, G.L., Tooth, S., Entwistle, N., 2018b. Morphodynamics of bedrock-influenced dryland rivers during extreme floods: insights from the Kruger National Park, South Africa. Geological Society of America Bulletin, 130, in press.

Milan, D.J., Heritage, G., Tooth, S. 2018c. Kruger National Park Rivers LiDAR data 2012. Centre for Environmental Data Analysis. Available at: http://catalogue.ceda.ac.uk/uuid/a2e82c7f92dc4f389a7fb7e4e6629c9e

Neal, J.C., Fewtrell, T.J., Bates, P.D., Wright, N.G., 2010. A comparison of three parallelisation methods for 2D flood inundation models. Environmental Modelling & Software, 25: 398-411.

Néelz, S., Pender, G., 2013. Delivering benefits thorough evidences: Benchmarking the Latest Generation of 2D Hydraulic Modelling Packages. Report—SC120002.

Nicholas, A.P., 2005. Cellular modelling in fluvial geomorphology. Earth Surface Processes and Landforms 30, 645-649.

Nicholas, A.P., 2010. Reduced-complexity modelling of free bar morphodynamics in alluvial channels: Journal of Geophysical Research - Earth Surface, 115 (F4).

Obasi, G.O.P., 2005. The impacts of ENSO in Africa. In Low, P.S. (Ed.), Climate Change and Africa, Cambridge: Cambridge University Press, pp. 218-230.

Rountree, M.W., Rogers, K.H., Heritage, G.L., 2000. Landscape state change in the semi-arid Sabie River, Kruger National Park, in response to flood and drought. South African Geographical Journal 82, 173-181.

Saint-Laurent, D., 2004. Palaeoflood hydrology: an emerging science. Progress in Physical Geography 28, 531-543.

Smith, A.M., 1992. Palaeoflood hydrology of the lower uMgeni River from a reach south of the Indaba Dam, Natal. South African Geographical Journal 74, 63-68.

Stear, W.M. 1985., Comparison of the bedform distribution and dynamics of modern and ancient

sandy ephemeral flood deposits in the southwestern Karoo region, South Africa. Sedimentary Geology 45, 209-230.

Steffen,W., Rockström,J., Richardson, K., Lenton, T.M., Folke,C., Liverman, D., Summerhayes, C.P., Barnosky, A.D., Cornell, S.E., Crucifix,M., Donges,J.F., Fetzer, I., Lade, S.J., Scheffer, M., Winkelmann, R., Schellnhuber, H.J., 2018. Trajectories of the Earth System in the Anthropocene, PNAS, in press.

Tooth, S., 2000. Process, form and change in dryland rivers: a review of recent research. Earth-Science Reviews 51, 67-107.

Tooth, S., 2013. Dryland fluvial environments: assessing distinctiveness and diversity from a global perspective. In: Shroder J, Wohl EE. (Eds.), Treatise on Geomorphology, Academic Press, San Diego, CA, v. 9, Fluvial Geomorphology, p. 612-644.

Tooth, S., Hancox, P.J., Brandt, D., McCarthy, T.S., Jacobs, Z., Woodborne, S.M., 2013. Controls on the genesis, sedimentary architecture, and preservation potential of dryland alluvial successions in stable continental interiors: insights from the incising Modder River, South Africa. Journal of Sedimentary Research 83, 541-561.

Tooth, S., McCarthy, T.S., 2004. Anabranching in mixed bedrock-alluvial rivers: the example of the Orange River above Augrabies Falls, Northern Cape Province, South Africa. Geomorphology 57, 235-262.

Tooth, S., McCarthy, T.S., Brandt, D., Hancox, P.J., Morris, R., 2002. Geological controls on the formation of alluvial meanders and floodplain wetlands: the example of the Klip River, eastern Free State, South Africa. Earth Surface Processes and Landforms 27, 797-815.

United Nations 2016. United Nations Decade: For Deserts and the fight against desertification. http://www.un.org/en/events/desertification_decade/whynow.shtml

van Niekerk, A.W., Heritage, G.L., Moon, B.P., 1995. River classification for management: the geomorphology of the Sabie River. South African Geographical Journal 77, 68-76.

Wang, L., D'Odorico, P.D., Evans, J.P., Eldridge, D.J., McCabe, M.F., Caylor, K.K., King, E.G.,

2012. Dryland ecohydrology and climate change: critical issues and technical advances. Hydrology and Earth System Science 16, 2585-2603.

Werner, M.G.F., Hunter, N.M., Bates, P.D., 2005. Identifiability of distributed floodplain roughness values in flood extent estimation. Journal of Hydrology 31, 139-157.

Williams, G.P., 1983. Paleohydrological methods and some examples from Swedish fluvial environments I. Cobble and boulder deposits. Geografiska Annaler, Series A 65, 227-243.

Wohl, E., David, G.C., 2008. Consistency of scaling relations among bedrock and alluvial channels. Journal of Geophysical Research: Earth Surface 113(F4).

Wohl, E., Merritt, D.M., 2008. Reach-scale channel geometry of mountain streams. Geomorphology 93, 168-185.

Womack, W.R., Schumm, S.A., 1977. Terraces of Douglas Creek, northwestern Colorado: an example of episodic erosion. Geology 5, 72-76.

Woodward, J.C., Tooth, S., Brewer, P.A., Macklin, M.G., 2010, The 4th International Palaeoflood Workshop and trends in palaeoflood science. Global and Planetary Change 70, 1–4.

Zawada, P.K., 1994. Palaeoflood hydrology of the Buffels River, Laingsburg, South Africa: was the 1981 flood the largest? South African Journal of Geology 97, 21-32.

Zawada, P.K., 1996. Palaeoflood Hydrology of Selected South African Rivers. PhD thesis (unpublished), University of Port Elizabeth.

Zawada, P.K., 2000. Slackwater sediments and paleofloods: their significance for Holocene paleoclimatic reconstruction and flood prediction. In: Partridge, T.C., Maud, R.R. (Eds.), The Cenozoic of Southern Africa, Oxford University Press, New York, 198–206.

Zawada, P.K., Hattingh, J., van Bladeren, D., 1996. Palaeoflood hydrological analysis of selected South African rivers. Pretoria: Water Research Commission Report 509/1/96.

Zawada, P.K., Smith, A.M., 1991. The 1988 Orange River flood, Upington region, Northwestern Cape Province, RSA. Terra Nova 3, 317–324.

649

Table 1. Rating equations and discharge range estimates for the Cyclone Dando floods in January 2012.

River	Site	Rating equation	R^2	Mean ($m^3 s^{-1}$)	Min ($m^3 s^{-1}$)	Max ($m^3 s^{-1}$)
Sabie upstream	S1	994.17 x - 252681	0.89	5423	5322	5474
	S2	799.15 x - 196814	0.88	5291	5072	5426
	S3	718.00 x - 162309	0.89	5129	5021	5236
	S4	807.62 x - 174412	0.87	5041	4959	5199
	S5	1414.60 x - 285616	0.99	5096	4649	5237
	S6	860.55 x - 157470	0.92	5174	5045	5258
	S7	708.16 x - 113191	0.94	4470	4364	4644
	S8	721.61 x - 106722	0.91	4550	4262	4764
Sabie downstream	S1	1051.30 x - 265900	0.94	5366	5298	5504
	S2	728.49 x -178469	0.98	5484	5378	5519
	S3	785.25 x - 176913	0.86	5352	5295	5465
	S4	1131.50 x - 244936	0.81	5237	5102	5372
	S5	1414.60 x - 285616	0.99	5630	5372	5709
	S6	896.86 x - 163283	0.88	5237	5156	5506
	S7	706.59 x - 112199	0.96	5095	5024	5236
	S8	686.98 x - 101047	0.86	4611	4404	4714
Olifants upstream	O1	1908.90 x - 378047	1	14423	14041	14614
	O2	2453.20 x - 507757	0.94	14407	13548	15020
	O3	2473.70 x - 450161	1	15637	13905	16379
	O4	3526.90 x - 619833	0.97	16772	16067	17478
	O5	1984.50 x - 297692	0.97	15859	15462	16454
Olifants downstream	O1	2118.50 x - 419168	0.99	15125	14701	15336
	O2	2726.30 x - 561512	0.94	15264	14010	15809
	O3	2819.00 x - 513987	0.98	14576	13166	15985
	O4	2950.10 x - 511883	1	16185	15595	16480
	O5	1766.60 x - 260630	0.98	16726	15843	17963

List of Figures

Fig. 1. A) Location of the Sabie and Olifants rivers and the Kruger National Park (KNP) in northeastern South Africa. Red boxes indicate the extent of the study reaches inside the KNP. B) and C) Flood strandline survey sites on the Sabie River and Olifants Rivers. The coordinate system in B) and C) is WGS84 UTM36S.

Fig. 2. Photographs from sites on the Sabie and Olifants rivers showing examples of the diverse channel types found in the KNP, and the impacts and preserved evidence of the 2012 Cyclone Dando floods: A) mixed braided type (Sabie River, flow direction from top to bottom); B) cohesive mixed anastomosed type (Sabie River, flow direction from bottom to top); C) bedrock anastomosed type (Sabie River, flow direction from top to bottom); D) example of the extensive stripping that occurred along many reaches of the Olifants river (flow direction from top to bottom, photograph courtesy of S. Woodborne); E), F) and G) typical strandline evidence recorded on the Sabie and Olifants rivers in the KNP, including examples of organic debris accumulations (flow direction is from left to right in E, and bottom to top in F and G); H) plastic drinks bottle embedded within a strandline, showing a 'Best Before' (BB) date of 4th July 2012. Given the limited shelf life of such products, this BB date implies that strandline would have been formed in the months preceding the survey (i.e. during the January 2012 floods) and not in earlier (pre-2011/2012) flood events. In G), note the considerable distance and elevation of the strandline from the low flow discharge (just visible on far middle right). In general, we surveyed finer material such as that showed in G, taking the highest elevation debris line as the datum.

Fig. 3. Surveyed flood strandline and simulated water surface elevations for the survey sites on: A) the Sabie River, for the high flow simulation of 5000 $m^3 s^{-1}$; and B) the Olifants River, for the high flow simulation of 15 000 $m^3 s^{-1}$.

Fig. 4. Surveyed flood strandline position (red dots) and simulated inundation extent on: A) the Sabie River, for the high flow simulation of 5000 $m^3 s^{-1}$; and B) the Olifants River, for the high flow simulation of 15 000 $m^3 s^{-1}$. The greyscale indicates water elevation for the flood peak simulations.

Fig. 5. Modelled discharge variation for the Cyclone Dando floods in January 2012 along the: A) Sabie River; and B) Olifants River. Bars indicate maximum and minimum discharge estimates (see Table 1); in some instance, the range in estimates is smaller than the plot symbol.

Fig. 6. Annual maximum flows on the: A) Sabie River at Lower Sabie Rest Camp (Station X3H015), located near the downstream end of the study reach; and B) Olifants Rivers at Mamba (Station B7H015), located near the upstream end of the study reach (Source: Department of Water Affairs and Forestry). M = missing data, Q = data not audited, A = above rating. It should be noted that some of the peaks are estimates rather than measurements from actual gauge records, as gauges are often damaged during the extreme flows. The 2000 flood for the Sabie River was estimated at 9400 $m^3 s^{-1}$, through extending weir rating relations to local flood levels, by the Department of Water Affairs and Forestry, and was larger than the Heritage et al. (2004) estimate of 6000-7000 $m^3 s^{-1}$.

Fig. 7. A) Extreme flood estimates for southern African rivers (after Kovacs 1988), incorporating the estimates for the Sabie and Olifants river floods of January 2012, as derived from the results of this study.

List of Tables

Fig 1

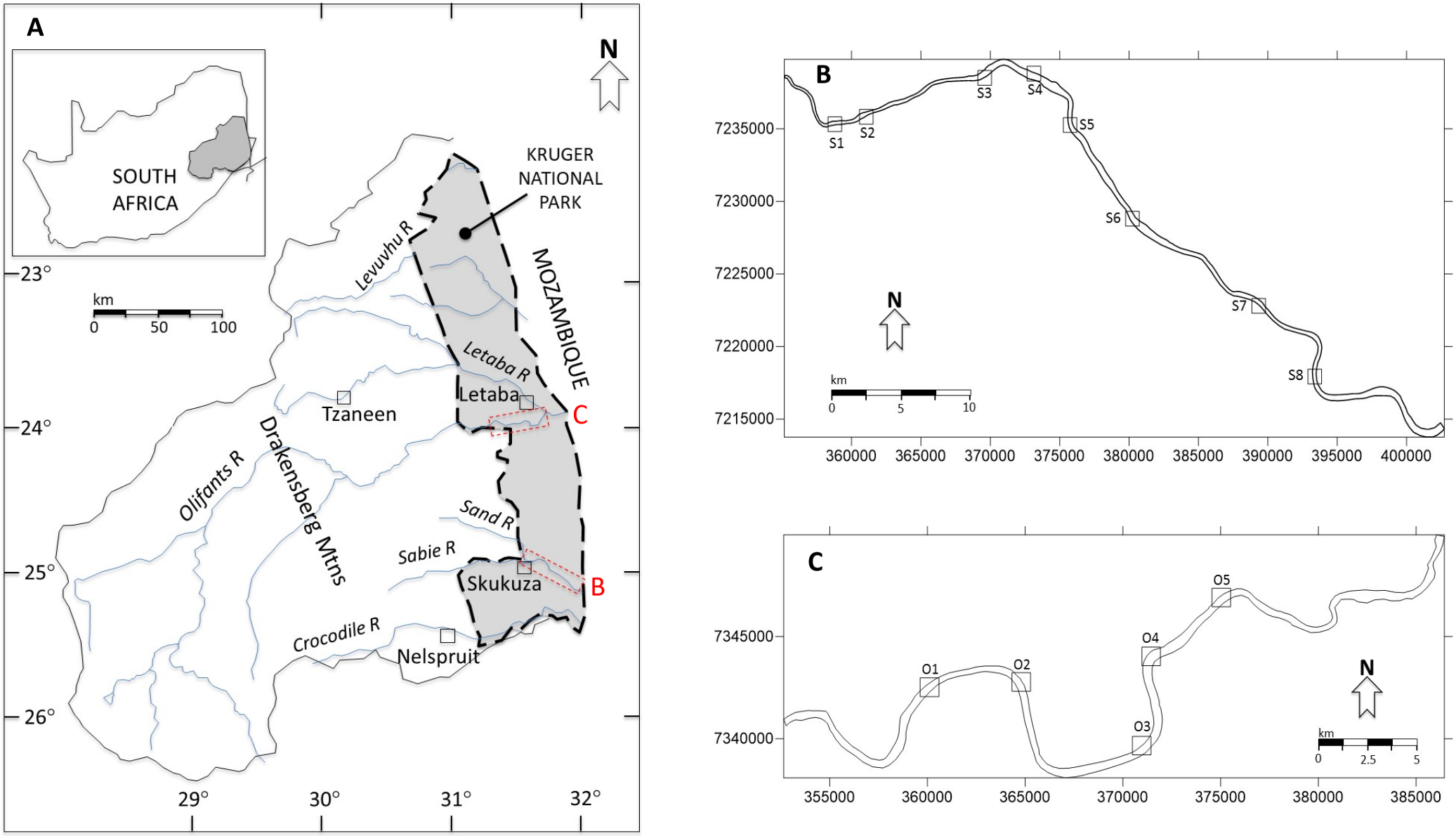
A
N
SOUTH AFRICA
KRUGER NATIONAL PARK
MOZAMBIQUE
Levuvhu R
Letaba R
Letaba
Tzaneen
Olifants R
Drakensberg Mtns
Sand R
Sabie R
Skukuza
Crocodile R
Nelspruit
B
C
km
0 50 100
23°
24°
25°
26°
29°
30°
31°
32°
B
S1
S2
S3
S4
S5
S6
S7
S8
7235000
7230000
7225000
7220000
7215000
360000 365000 370000 375000 380000 385000 390000 395000 400000
km
0 5 10
C
O1
O2
O3
O4
O5
7345000
7340000
355000 360000 365000 370000 375000 380000 385000
km
0 2.5 5

Fig 2

A

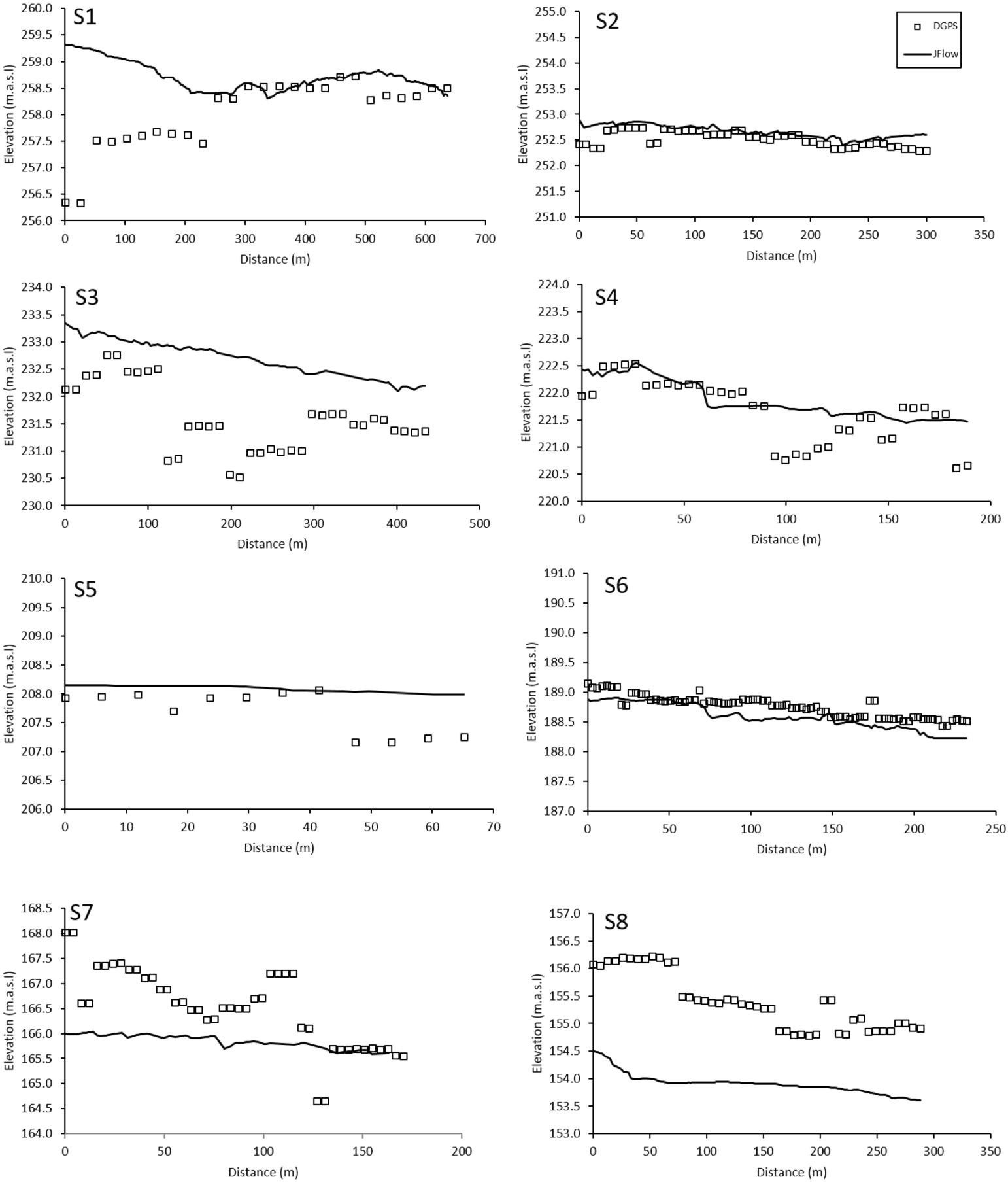
S1
Elevation (m.a.s.l)
Distance (m)
S2
DGPS
JFlow
Elevation (m.a.s.l)
Distance (m)
S3
Elevation (m.a.s.l)
Distance (m)
S4
Elevation (m.a.s.l)
Distance (m)
S5
Elevation (m.a.s.l)
Distance (m)
S6
Elevation (m.a.s.l)
Distance (m)
S7
Elevation (m.a.s.l)
Distance (m)
S8
Elevation (m.a.s.l)
Distance (m)

Fig 3A

B

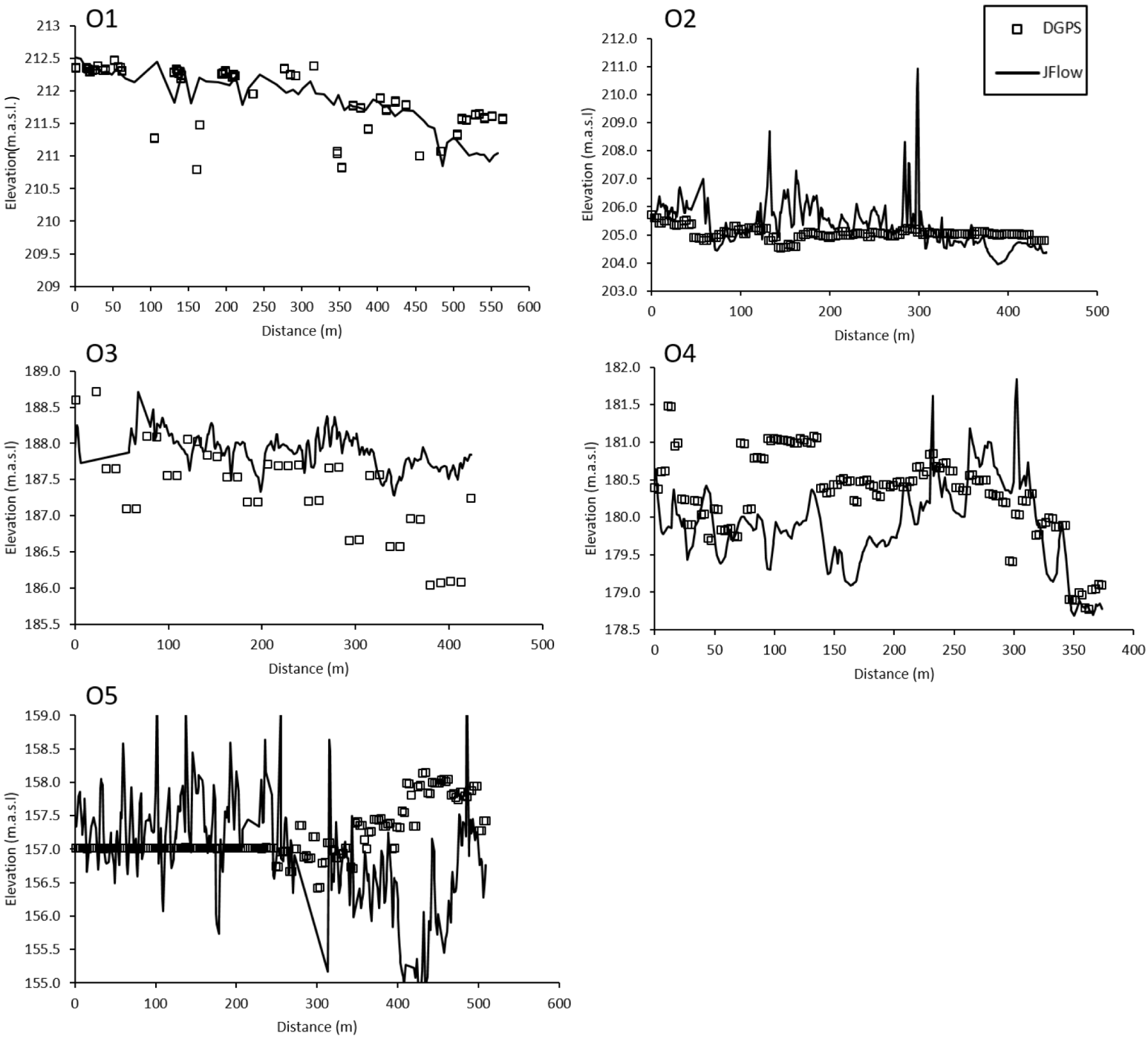
O1
Elevation(m.a.s.l.)
213
212.5
212
211.5
211
210.5
210
209.5
209
0 50 100 150 200 250 300 350 400 450 500 550 600
Distance (m)
O2
DGPS
JFlow
Elevation (m.a.s.l)
212.0
211.0
210.0
209.0
208.0
207.0
206.0
205.0
204.0
203.0
0 100 200 300 400 500
Distance (m)
O3
Elevation (m.a.s.l)
189.0
188.5
188.0
187.5
187.0
186.5
186.0
185.5
0 100 200 300 400 500
Distance (m)
O4
Elevation (m.a.s.l)
182.0
181.5
181.0
180.5
180.0
179.5
179.0
178.5
0 50 100 150 200 250 300 350 400
Distance (m)
O5
Elevation (m.a.s.l)
159.0
158.5
158.0
157.5
157.0
156.5
156.0
155.5
155.0
0 100 200 300 400 500 600
Distance (m)

Fig 3B

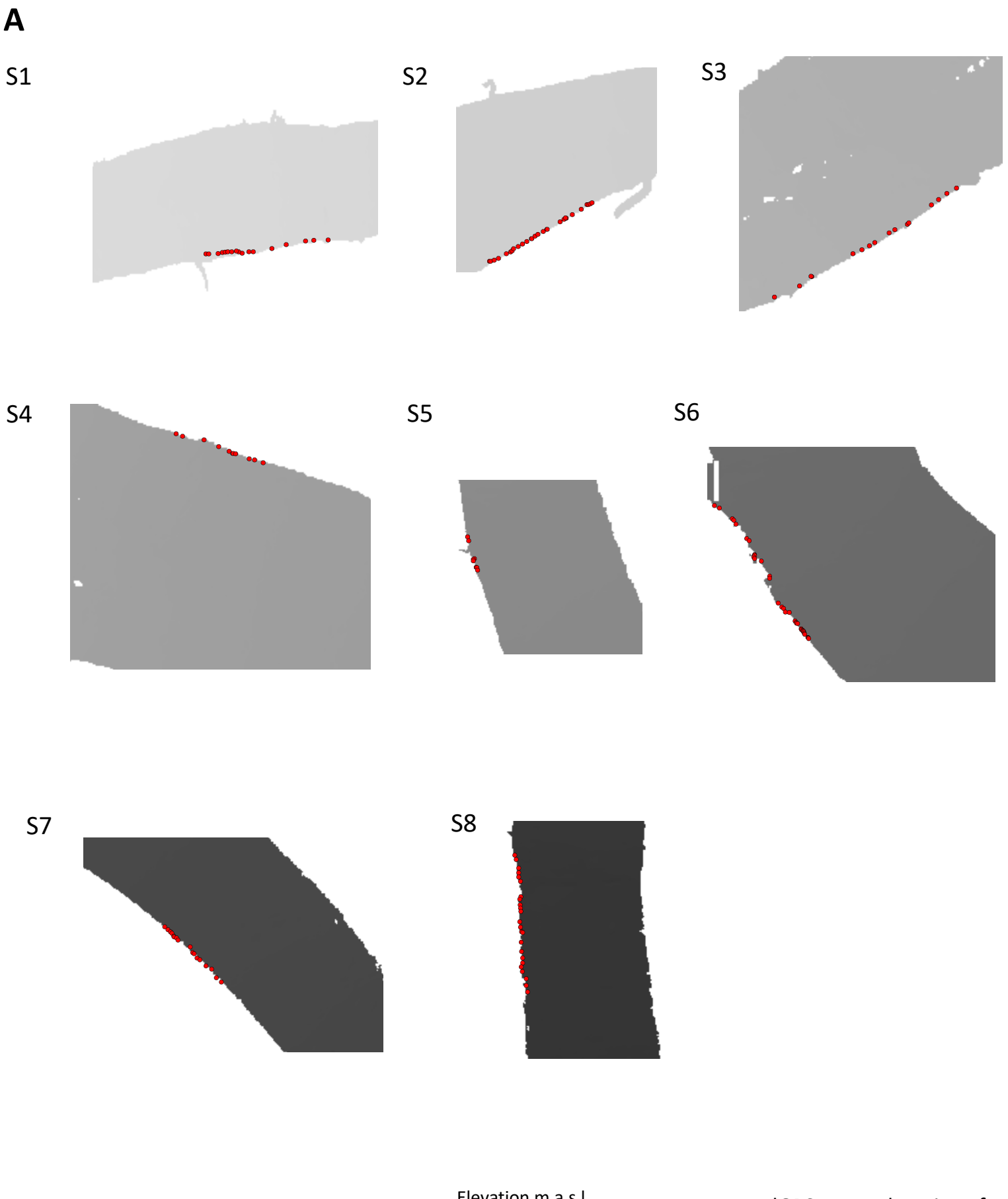
A
S1
S2
S3
S4
S5
S6
S7
S8
m
0
100
200
300
400
Elevation m.a.s.l.
120
145
170
195
220
245
270
dGPS survey locations for strandline debris

Fig 4A

B

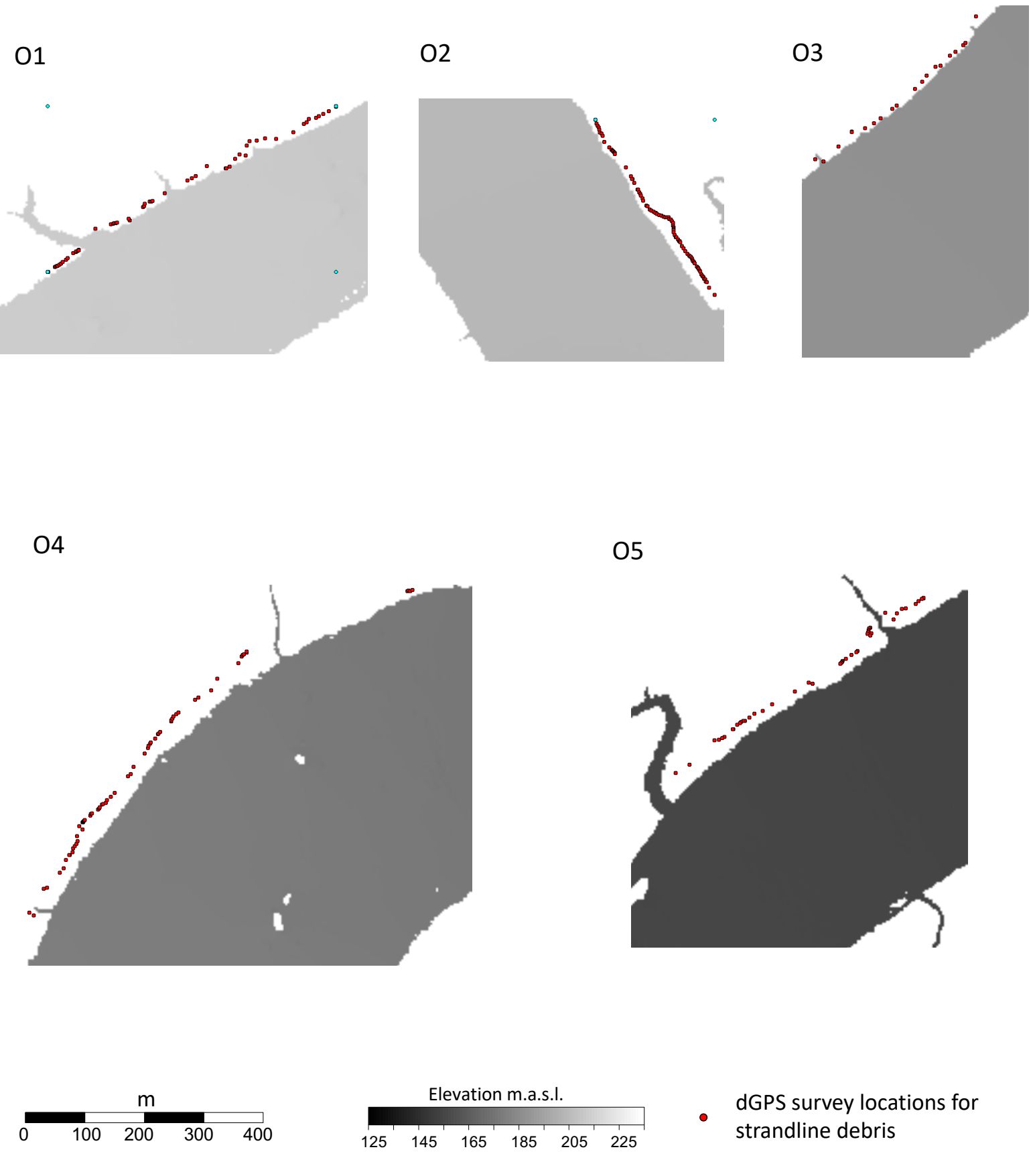
O1
O2
O3
O4
O5
m
0
100
200
300
400
Elevation m.a.s.l.
125
145
165
185
205
225
dGPS survey locations for strandline debris

Fig 4B

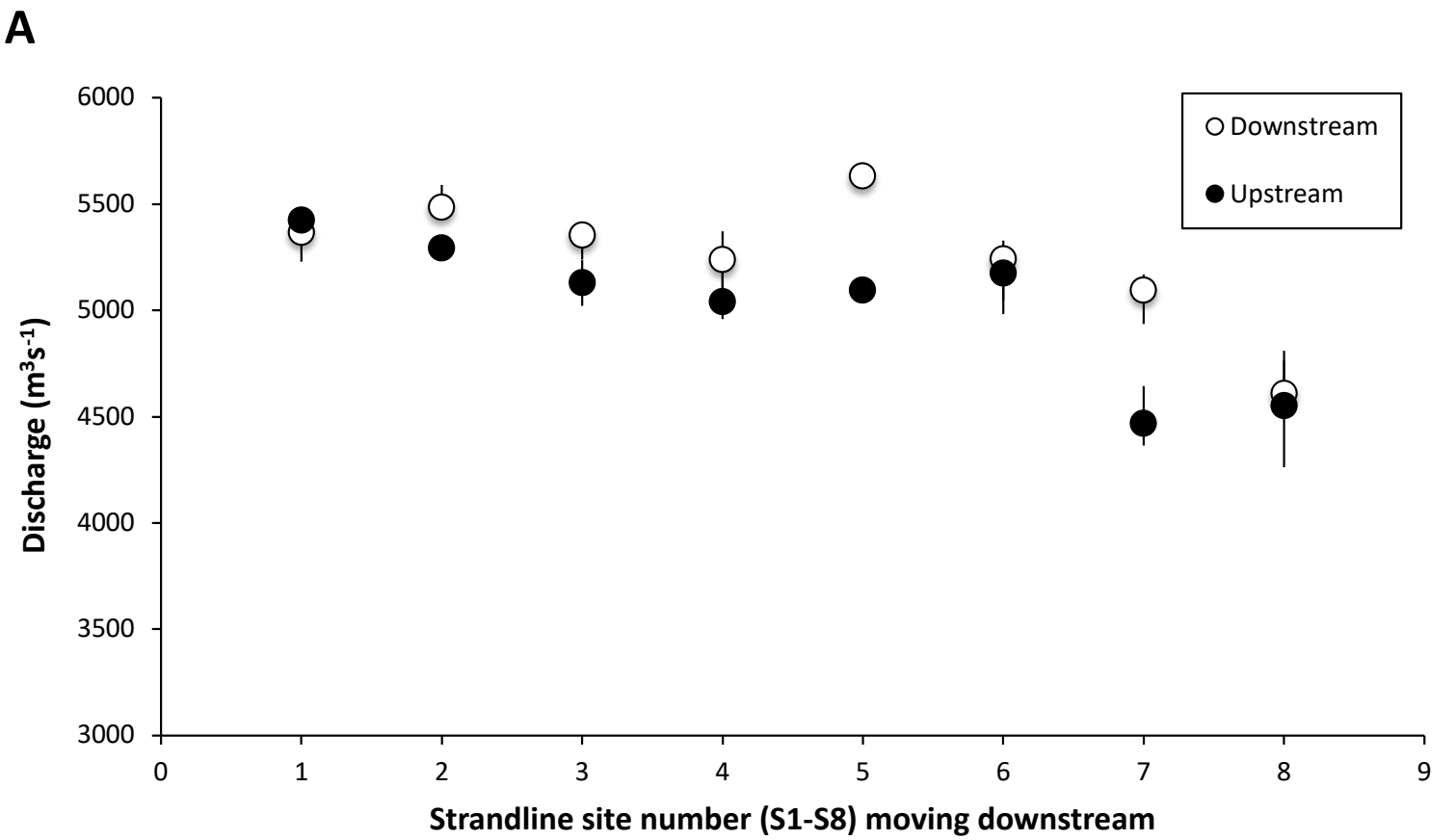
A
6000
5500
5000
4500
4000
3500
3000
Discharge (m³s⁻¹)
0
1
2
3
4
5
6
7
8
9
Strandline site number (S1-S8) moving downstream
Downstream
Upstream

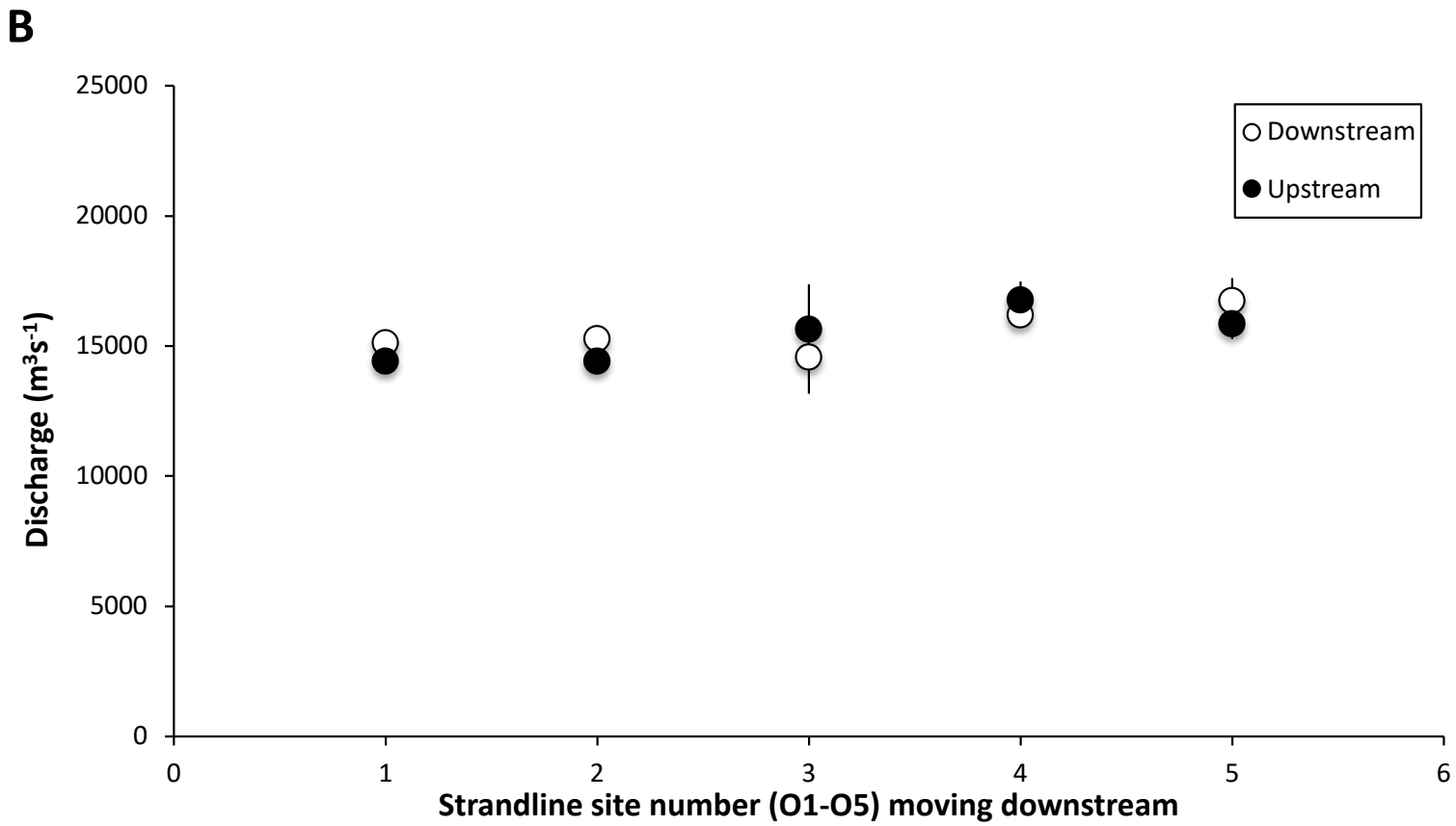
B
25000
20000
15000
10000
5000
0
Discharge (m³s⁻¹)
0
1
2
3
4
5
6
Strandline site number (O1-O5) moving downstream
Downstream
Upstream

Fig 5

A

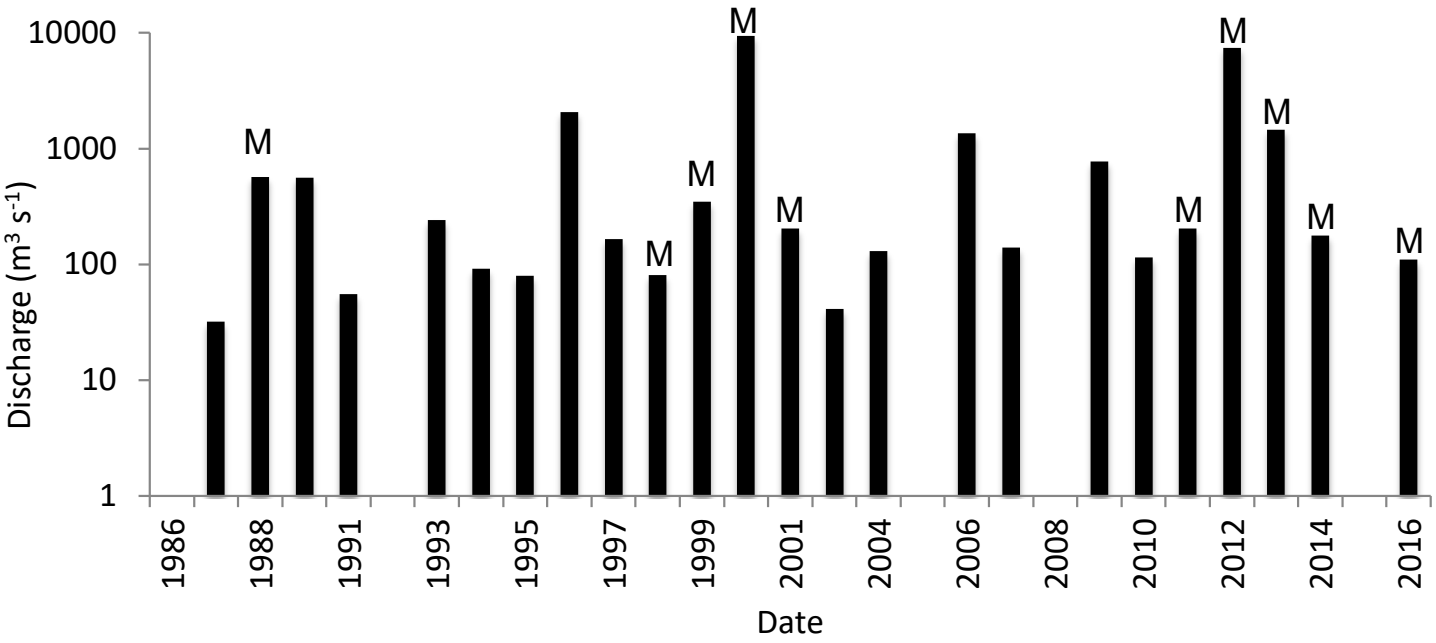
10000
1000
100
10
1
Discharge (m³ s⁻¹)
M
1986
1988
1991
1993
1995
1997
1999
2001
2004
2006
2008
2010
2012
2014
2016
Date

B

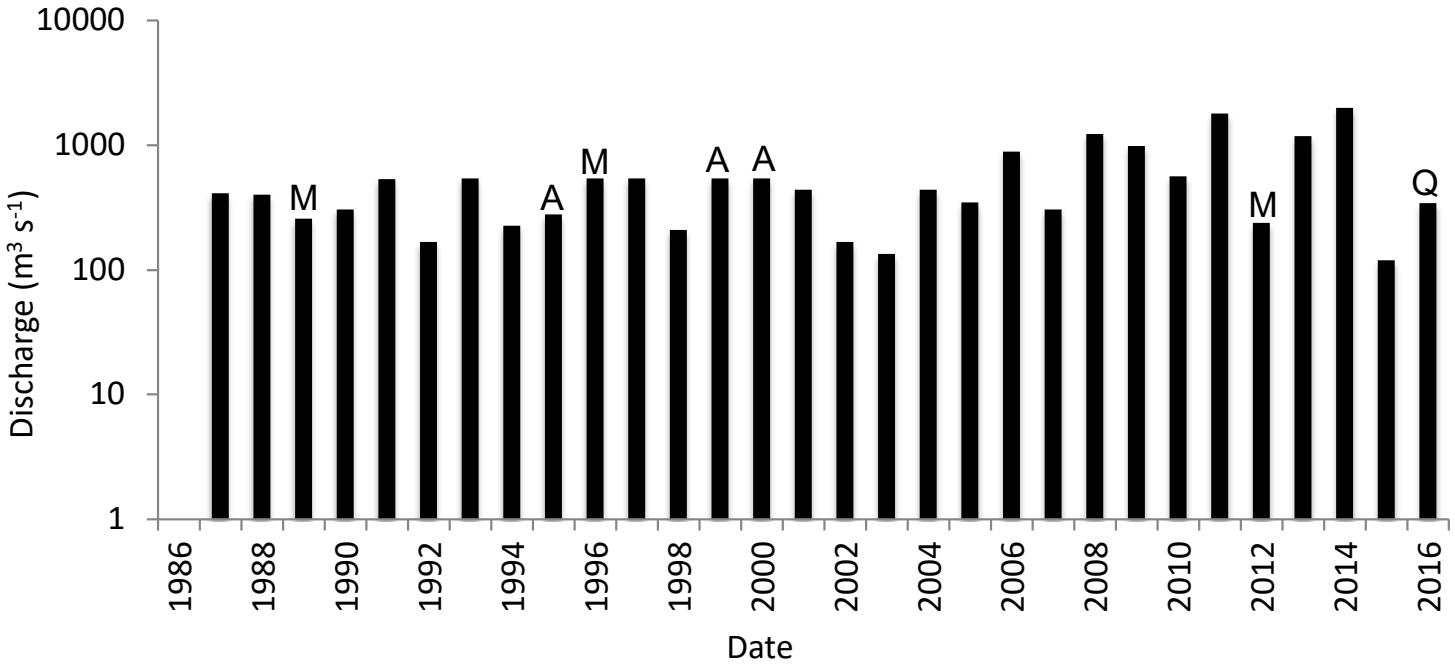
10000
1000
100
10
1
Discharge (m³ s⁻¹)
M
A
M
A
A
M
Q
1986
1988
1990
1992
1994
1996
1998
2000
2002
2004
2006
2008
2010
2012
2014
2016
Date

Fig 6

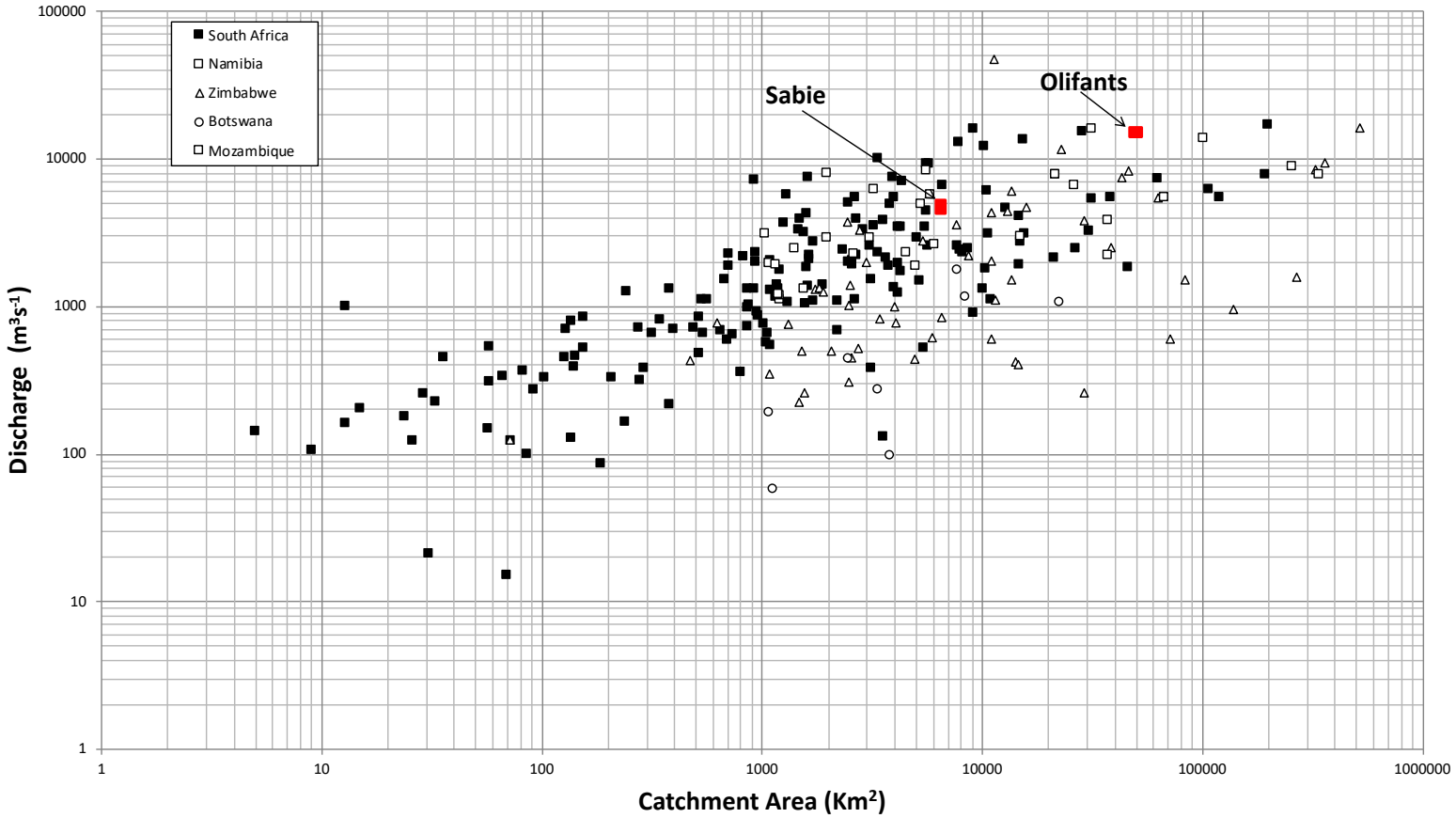
South Africa
Namibia
Zimbabwe
Botswana
Mozambique
Sabie
Olifants
Discharge (m³s⁻¹)
Catchment Area (Km²)
100000
10000
1000
100
10
1
1
10
100
1000
10000
100000
1000000

Fig 7